Source Localization with Feedback Beamforming

Itay Yehezkel Karo, Tsvi G. Dvorkind, and Israel Cohen, *Fellow, IEEE*

***Abstract*—State-of-the-art array processing methods, ranging from high-order statistics to adaptive configuration, require costly computing efforts in pursuit for spatial performance improvement. A feedback based approach is introduced in the context of localization, featuring low complexity and high spatial performance in the excess of integrating a transmitter to the array. In the proposed scheme, a signal is continuously re-transmitted between the array and the target of interest. Considering ideal scenarios, the feedback beamformer virtually achieves an infinite aperture, increasing the available spatial information about the target and significantly improves the array's spatial performance. Using a traditional beamforming performance analysis, the beamwidth, peak to side-lobe ratio, array directivity and white noise sensitivity are evaluated for the feedback based array. A significant improvement in all aspects is shown, while thoroughly discussing the conditions for enhanced performance. As a practical and robust implementation of the feedback-based localization concept, an application of low estimation errors sensitivity, is presented and analyzed.**

***Index Terms*—Beamforming, beampattern, cooperative beamforming, source localization, spatial array processing, spatial IIR.**

I. Introduction

THE general field of array processing has been thoroughly studied throughout several decades. The array sensors' spatial diversity enables the extraction of spatial information about impinging signals, thus laying the ground for wide range of applications, such as localizing a transmitting source [1], [2], blindly separating mixtures of impinging signals [3], improving signal to noise ratio (SNR) [4], and many more.

A uniform linear array (ULA) has always been a point of interest, due to its simplicity of analysis [5], [6]. The array size and the number of its elements (N) have significant influence on the obtained array performance, such as SNR improvement, spatial separation capabilities and its spatial response's degrees of freedom (DOF). For example, the influential MUSIC algorithm [7] enables the localization of signals arriving from up to $N-1$ distinctive directions of arrival (DOA), by projecting the array manifold onto the noise subspace.

Manuscript received November 30, 2019; revised July 22, 2020; accepted October 13, 2020. Date of publication November 6, 2020; date of current version January 20, 2021. The associate editor coordinating the review of this manuscript and approving it for publication was Dr. Paolo Braca. This work was supported in part by the Israel Science Foundation under Grant 576/16, and in part by the ISF-NSFC joint research program under Grant 2514/17. *(Corresponding author: Itay Yehezkel Karo.)*

Itay Yehezkel Karo and Israel Cohen are with the Andrew and Erna Viterby Faculty of Electrical Engineering, Technion – Israel Institute of Technology, Technion City, Haifa 3200003, Israel (e-mail: itayyeka@campus.technion.ac.il; icohen@ee.technion.ac.il).

Tsvi G. Dvorkind is with Rafael Advanced Defense Systems, Haifa 31021, Israel (e-mail: dvorkind@rafael.co.il).

Digital Object Identifier 10.1109/TSP.2020.3034719

In pursuit of spatial performance improvement, namely higher spatial separation and selectivity of arriving signals, many approaches were suggested. One approach, commonly referenced as "virtual arrays" [8]–[10] deals with the extraction of samples originated in sensors that do not really exist by using high (higher than 2) order statistics and manipulating multiple statistical cross-terms in order to estimate statistical characteristics of signals impinging on missing sensors. Using a similar approach, the $2q$-MUSIC algorithm [11], enables the use of N^{2q} "virtual elements", by calculating the q'th order statistics. Another approach, involving different array geometries, examined minimum redundancy arrays [12]–[15], aiming to reduce the spatial ambiguity. The basic concept was minimization of the inter-element spacing redundancy in order to increase the overall resolution. Adaptive processing schemes [16], [17], being a wide and active research area, were also suggested trying to adaptively estimate and suppress the noise component in impinging signals by minimization of the receiver's output energy with some constraints.

Pursuing other approaches to improve the array's spatial performance, ULA spatial array processing analogy to finite impulse response (FIR) [18] and the infinite impulse response (IIR) superior performance (e.g. narrower transition regions and higher sidelobes attenuation) gave rise to the question "what are the spatial domain processing methods which will be analogous to temporal domain IIR filtering?"

Achieving a spatial IIR response has also motivated other works. In [19] two methods were considered. The first one was to estimate the time of arrival (TOA) difference between two consecutive sensors and to synthetically generate the recursive part of the IIR filter, entirely in the time-domain. The second approach suggested to consider overlapping subsets of one large ULA as a finite approximation to an infinite array. Surely, the former approach heavily relies on the accuracy of the delay estimation and the latter approach does not achieve a recursive spatial response. In both cases, there is no true spatial feedback between the array and the source of interest. Also, ultra-wideband (UWB) filters, which sample spatial snapshots of the signal and recursively process it in the temporal domain were designed in [20], using the 2D spatio-temporal plane wave representation as a straight line angled according to the DOA.

In this contribution, we present a low-complexity sensor array processing approach which achieves the desired spatial domain exclusive IIR-like beampattern, while avoiding any temporal processing of the signal. To this end, we arbitrarily choose to formulate the problem in the context of localization, hence our goal is to estimate the direction and the range of some target of interest.

The novelty, compared to traditional array processing, is the incorporation of a spatial feedback, which we prove to be the spatial domain equivalent of temporal domain IIR filtering. Assuming the target of interest has a mirror-like behaviour (i.e. reflects its impinging signals), the spatial feedback between the array and the target is created by continuously re-transmitting a synthesized version of the impinging signal (and its reflections) to the target. Note that the initial stimulus can be generated by the target or the array itself. In the text to follow, we assume this is the latter. Furthermore, as opposed to the passive target case (i.e., a target which merely reflects the impinging signal), one may consider a cooperative target, which receives, enhances and re-transmits the signal back to the array.

The outline of this paper is as follows. We first formulate the classic spatial beamforming setup in Section II. Then, in Section III, we propose our novel feedback-based architecture, and formulate its spatial response. Searching for localization performance maximization, Section IV discusses the information-theory related considerations for the array configuration, utilizing the Fisher Information Matrix (FIM) in the context of the target's range and DOA estimation. In Section V, we evaluate some key features of the proposed beamforming with feedback. Specifically, we compute the array beamwidth, its peak-to-sidelobe ratio and the array directivity, showing significant improvement compared to traditional beamforming without spatial feedback. In Section VII, we simulate the proposed processing scheme, and emphasize its sensitivity to range errors. We then suggest a strategy which mitigates this sensitivity. Finally, concluding remarks are given in Section VIII.

II. Beamforming

In this section, a brief overview on ULA beamforming and its resemblance to FIR filter design are presented. Consider an N-element ULA with inter-element spacing δ, where its n'th sensor is positioned at $\boldsymbol{p}_n$, for $n = 0, \ldots, N-1$. We set $\boldsymbol{p}_0$ as the axis reference point and assume that the target of interest is positioned at $\boldsymbol{p}_{\mathrm{t}}$. Focusing on a far field localization problem, DOA and target range are to be estimated. Without loss of generality, aiming to simplify the exposition, we assume 2D planar problem, where DOA is described by a single angle θ_{d}, measured from the array's broadside. For simplicity, we assume an anechoic environment, an array of identical omni-directional sensors and a stationary target of interest. Inspired by radar based applications, we also place a transmitter at $\boldsymbol{p}_0$, assuming the transmitted signal s, is reflected back from the target and re-impinges the array, with a total time delay of $\tau_{\mathrm{pd}} = 2R/c$ seconds, where $R = \|\boldsymbol{p}_{\mathrm{t}} - \boldsymbol{p}_0\|$ is the target's range and c represents the propagation velocity of the signal in the medium. In this work, we use the following conventions; vectors and matrices are denoted by lower and upper case bold italic letters respectively. v_i and A_{ij} are the i-th element of the vector $\boldsymbol{v}$ and the i,j-th element of the matrix $\boldsymbol{A}$. Also, $\boldsymbol{A}^T, \boldsymbol{A}^*$ and $\boldsymbol{A}^H$ are the transpose, conjugate and Hermitian transpose of the matrix $\boldsymbol{A}$ respectively.

Let $x_n(t)$ be the measured signal at the n'th sensor

$$x_n(t) = gs\left(t - \tau_{pd} - \tau_n\right), \tag{1}$$

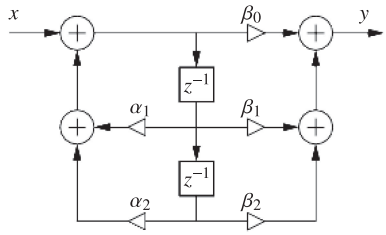

Fig. 1. Direct form II 2^{nd} order IIR architecture.

where $\tau_n = n\delta\cos(\theta_{\mathrm{d}})/c$ represents the time difference of arrival between the n'th sensor and the reference sensor and g, being a scalar in an anechoic environment, is the channel's gain, related to both propagation and the target's radar cross section (RCS). Defining $\boldsymbol{x}(t) \triangleq [x_0(t) \ldots x_{N-1}(t)]^T$ and its Fourier transform, $\mathrm{X}(\omega) \triangleq [X_0(\omega), \ldots, X_{N-1}(\omega)]^T$, one may write

$$\mathrm{X}(\omega) = g\boldsymbol{d}(\omega)\,\mathrm{S}(\omega)\exp\left(-j\omega\tau_{pd}\right)$$

where $S(\omega)$ is the Fourier transform of $s(t)$ and $\boldsymbol{d}(\omega)$ denotes the steering vector whose n'th element is

$$d_n(\omega) = \exp\left(-j\omega\tau_n\right). \tag{2}$$

Denoting the beamformer's weights as $\boldsymbol{\beta}(\omega)$ and the beamformer's output as z, we express the latter in the frequency domain

$$Z(\omega) = g\boldsymbol{\beta}^H(\omega)\boldsymbol{d}(\omega)\,\mathrm{S}(\omega)\exp\left(-j\omega\tau_{pd}\right). \tag{3}$$

Defining the electric phase to be

$$\theta = \omega\delta\cos(\theta_{\mathrm{d}})/c, \tag{4}$$

we rewrite (3) as

$$Z(\omega) = g\mathrm{S}(\omega)\exp\left(-j\omega\tau_{pd}\right)\sum_{n=0}^{N-1}\beta_n^*(\omega)\exp\left(-jn\theta\right),$$

hence in the ULA case, aiming for a desired spatial response, the weights vector $\boldsymbol{\beta}(\omega)$ configuration is mathematically equivalent to an FIR filter design [6], [18]. Assuming narrowband stimuli signals, we suppress ω dependency in the notation throughout the rest of this paper, where possible.

In standard radar signal processing schemes, a waveform is transmitted to, and reflected from the target of interest. Then, the reflected signal is processed by the radar reception array in order to estimate the target's dynamics (e.g., DOA, range, velocity etc.). As opposed to the standard scheme, we suggest a continuous re-transmission of the signal and its echoes back to the platform, generating a spatial feedback loop between the array and the target. Another deviation from traditional radar processing, used to simplify the exposition, is using continuous-wave (CW) stimuli, rather than using pulse based signals.

III. Feedback Beamforming

In this section, a feedback-based architecture is proposed for spatial signal processing. Inspired by time domain "Direct form II" IIR filter design (see Fig. 1), we propose to use the same concept in the spatial domain. The suggested feedback

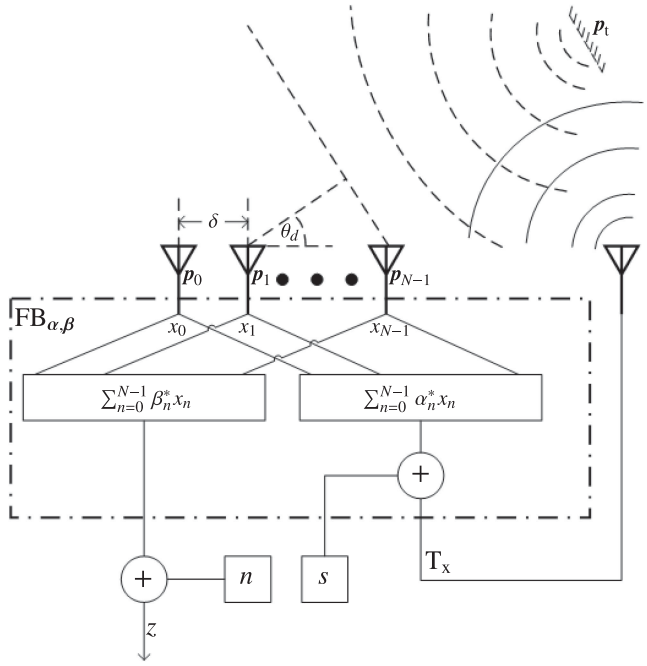

Fig. 2. The proposed feedback beamformer. The spatial feedback is obtained by continuous re-transmission of T_x to the target at $\boldsymbol{p}_t$. We designate the feedback beamformer block (dashed line) for later use.

beamformer (FB) architecture, where the output signal (z) is synthesized using weights $\boldsymbol{\beta}$ and the weights $\boldsymbol{\alpha}$ synthesize the feedback transmission (T_x), is presented in Fig. 2. The beamformer's output and the feedback signal are synthesized using two independently configured beamformers, s is the system's stimulus and an additive noise (n) is assumed at the array's output. Also, the FB block is marked (dashed line) for later use. Note that setting $\boldsymbol{\alpha} = 0$ (i.e., cancelling the feedback) degenerates the system to a plain delay-and-sum (DS) beamformer.

A. Obtained Spatial Response

Time domain analysis of the proposed feedback based architecture, considering both propagation delay and attenuation, gives rise to

$$x_n(t) = g\left(s\left(t - \tau_{pd} - \tau_n\right) + \sum_{m=0}^{N-1} \alpha_m^* x_m\left(t - \tau_{pd} - \tau_n\right)\right), \quad (5)$$

where the first term on the right-hand-side (RHS) represents the contribution of the transmitted waveform $s(t)$ to the n'th array element and the second term represents the feedback contribution of the re-transmitted array signal to this same element. Expressing the Fourier transform of (5),

$$X_n = g\Bigg(\mathrm{S}\exp\left(-j\omega\left(\tau_{pd} + \tau_n\right)\right) + \sum_{m=0}^{N-1} \alpha_m^* \mathrm{X}_m \exp\left(-j\omega\left(\tau_{pd} + \tau_n\right)\right)\Bigg), \quad (6)$$

and its vector from,

$$\boldsymbol{X} = g\left(\mathrm{S} + \boldsymbol{\alpha}^H \boldsymbol{X}\right)\boldsymbol{d}\exp\left(-j\omega\tau_{pd}\right),$$

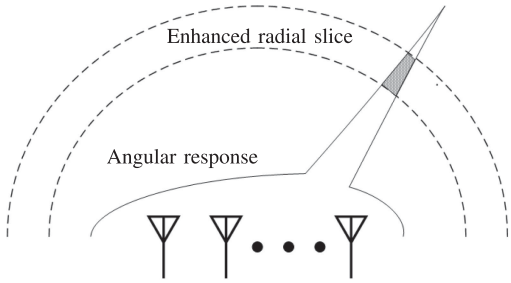

Fig. 3. Combining both radial selectivity and DOA-based selectivity allows to localize the target.

we find that it can be simplified to

$$\boldsymbol{X} = g\left(I - g\boldsymbol{d}\boldsymbol{\alpha}^H e^{-j\omega\tau_{pd}}\right)^{-1}\boldsymbol{d}\mathrm{S}\exp\left(-j\omega\tau_{pd}\right).$$

Then, denoting

$$\phi \triangleq \omega\tau_{pd}$$

as the round-trip signal propagation related electrical phase and using the Woodbury matrix identity [21], we find that

$$\boldsymbol{X} = \frac{g\boldsymbol{d}\exp\left(-j\phi\right)}{1 - g\boldsymbol{\alpha}^H\boldsymbol{d}\exp\left(-j\phi\right)}\mathrm{S}.$$

Let $z = \boldsymbol{\beta}^H\boldsymbol{x} + \mathrm{n}$ be the beamformer's output (see Fig. 2), with Fourier transform Z. Considering the noiseless case (i.e., $\mathrm{n} = 0$), the frequency response of the FB is

$$H_{\boldsymbol{\beta},\boldsymbol{\alpha}} \triangleq \frac{\mathrm{Z}}{\mathrm{S}} = \frac{g\boldsymbol{\beta}^H\boldsymbol{d}\exp\left(-j\phi\right)}{1 - g\boldsymbol{\alpha}^H\boldsymbol{d}\exp\left(-j\phi\right)}. \quad (7)$$

Note that this architecture achieves a controllable (via setting of $\boldsymbol{\beta}$ and $\boldsymbol{\alpha}$) and recursive (non-trivial denominator) spatial response. As will be shown, high directivity and narrow beamwidth are obtainable by a proper selection of the weights. Compared to traditional beamformers (i.e., without feedback), the performance improvement will be expressed in terms of increased aperture, narrower beamwidth and improved sidelobe attenuation. One may observe that opposed to traditional beamformers, the array response, $H_{\boldsymbol{\beta},\boldsymbol{\alpha}}$, is not only influenced by the impinging signal DOA, since it is also range selective due to its ϕ dependency. As demonstrated in Fig. 3, the combination of both angular and range selectivity enables the designer to enhance signals arriving from specific locations (grey area) rather than only specific directions.

IV. Fisher Information Matrix

A possible evaluation for the contribution of the presented feedback mechanism is to measure the additional information in the system. To this end, the FIM, denoted by $\boldsymbol{J}$, will now be calculated with respect to the DOA (θ_d) and range (ϕ) parameters. As the feedback-based transfer function (7) is expressed in the frequency domain, we rely on [22] to express the frequency domain FIM as well.

The $[k, l]$'th FIM element, may be expressed as

$$J_{k,l}(\boldsymbol{\eta}) = \Re\left\{\frac{1}{2\pi}\int_{-\omega_s/2}^{\omega_s/2}\frac{1}{\Phi(\omega)}\mathfrak{F}^*\left\{\frac{\partial z(t)}{\partial\eta_k}\right\}\mathfrak{F}\left\{\frac{\partial z(t)}{\partial\eta_l}\right\}d\omega\right\}$$

$$+\frac{T}{4\pi}\int_{-\omega_s/2}^{\omega_s/2}\frac{1}{\Phi^2(\omega)}\left(\frac{\partial\Phi(\omega)}{\partial\eta_k}\right)^*\frac{\partial\Phi(\omega)}{\partial\eta_l}d\omega \quad (8)$$

where $\boldsymbol{\eta}=[\theta_{\mathrm{d}},\phi]^T$ is the parameters vector, $\Re$ stands for the real-part extraction operator, $k,l\in\{1,2\}$, $\Phi(\omega)$ is the noise spectrum, $\mathfrak{F}$ is the Fourier transform operator, T is the measurement observation interval and ω_s is the signal bandwidth. For simplicity, $\mathrm{n}(t)$ is assumed to be white Gaussian with some constant power spectral density $\Phi(\omega)=\sigma^2$ and independent of the estimated parameters $\boldsymbol{\eta}$. Hence, the second term in the RHS of (8) vanishes. Assuming continuously differentiable functions, where order alteration of the Fourier transform and the differentiation operations is allowed, (8) simplifies to

$$J_{kl}(\boldsymbol{\eta})=\Re\left\{\frac{1}{2\pi\sigma^2}\int_{-\omega_s/2}^{\omega_s/2}\left(\frac{\partial\mathrm{Z}(\omega)}{\partial\eta_k}\right)^*\frac{\partial\mathrm{Z}(\omega)}{\partial\eta_l}d\omega\right\}. \quad (9)$$

Expressing the steering vector derivative with respect to θ_{d}, results in

$$\frac{\partial\boldsymbol{d}}{\partial\theta_{\mathrm{d}}}=\boldsymbol{A}\boldsymbol{d} \quad (10)$$

where $\boldsymbol{A}$ is an $N\times N$ diagonal matrix with

$$A_{ii}=-j\omega\frac{\partial\tau_i}{\partial\theta_{\mathrm{d}}}\ \ \forall i\in\{0\ldots N-1\}.$$

It is worth mentioning that (10) is relevant even for arbitrary arrays (not necessarily ULA) when smooth and slowly changing radiation patterns are assumed. In Appendix A we compute the FIM terms, concluding that

$$\begin{aligned}J_{11}&=J_{\theta_{\mathrm{d}}\theta_{\mathrm{d}}}\\&=\frac{1}{2\pi\sigma^2}\int_{-\omega_s/2}^{\omega_s/2}\frac{\left|g\boldsymbol{\beta}^H\boldsymbol{A}\boldsymbol{d}-g^2\boldsymbol{\beta}^H\boldsymbol{B}\boldsymbol{\alpha}^*\exp(-j\phi)\right|^2}{\left|1-g\boldsymbol{\alpha}^H\boldsymbol{d}\exp(-j\phi)\right|^4}\\&\quad\times|\mathrm{S}(\omega)|^2d\omega\\J_{22}&=J_{\phi\phi}\\&=\frac{1}{2\pi\sigma^2}\int_{-\omega_s/2}^{\omega_s/2}\frac{\left|g\boldsymbol{\beta}^H\boldsymbol{d}\right|^2}{\left|1-g\boldsymbol{\alpha}^H\boldsymbol{d}\exp(-j\phi)\right|^4}|\mathrm{S}(\omega)|^2d\omega.\end{aligned} \quad (11)$$

where $\boldsymbol{B}\triangleq\boldsymbol{d}\boldsymbol{d}^T\boldsymbol{A}-\boldsymbol{A}\boldsymbol{d}\boldsymbol{d}^T$. Aiming to maximize the FIM diagonal elements via denominator (i.e., $|1-g\boldsymbol{\alpha}^H\boldsymbol{d}\exp(-j\phi)|$) minimization, the optimal feedback weights are

$$\boldsymbol{\alpha}^*_{\mathrm{CB,opt}}=\frac{\boldsymbol{d}^*\exp(j\phi)}{\hat{g}\left\|\boldsymbol{d}\right\|^2}, \quad (12)$$

where $\hat{g}$ is the channel gain estimate. This choice of weights may be interpreted as a generalized version of the conventional beamformer (CB) [5]. Furthermore, setting $\boldsymbol{\beta}=\boldsymbol{\beta}_{\mathrm{CB,opt}}=\boldsymbol{\alpha}_{\mathrm{CB,opt}}$, is shown (see Appendix A) to nullify the FIM cross terms, such that $J_{12}=J_{\theta_{\mathrm{d}},\phi}=J_{21}=J_{\phi\theta_{\mathrm{d}}}=0$.

Note that setting the feedback weights as in (12) requires perfect knowledge of the target's range, since ϕ is range dependant. Also, the reader may notice that assuming $\hat{g}=g$, this choice of optimal weights nullifies the denominator of (7). Thus, theoretically, the FIM becomes infinite when the transfer function (7) is unstable due to positive and coherent feedback between the beamformer and the target. In practice, though, there will be unavoidable errors, and perfect knowledge of target's location and the channel gain is usually absent. In Section V, we quantify the effect of such errors and discuss its influence on the array performance.

V. Performance Analysis

In this section we analyze the suggested FB (see Fig. 2), considering some fundamental properties which are commonly used to asses array performance: Beamwidth, peak-to-sidelobe level, and directivity. Each property is then compared to traditional passive ULAs, showing that significantly improved performances are obtainable with spatial feedback integration.

A. Error terms

In the absence of accurately known parameters, we denote $\hat{\phi},\hat{\theta}$ to be the range and DOA related phase estimates respectively. Then, using the same weights as in (12) for both the feedback and output synthesis gives rise to

$$\boldsymbol{\beta}^*_{\mathrm{CB}}=\boldsymbol{\alpha}^*_{\mathrm{CB}}=\frac{\hat{\boldsymbol{d}}^*\exp\left(j\hat{\phi}\right)}{\hat{g}\left\|\hat{\boldsymbol{d}}\right\|^2}, \quad (13)$$

introducing the estimated steering vector

$$\hat{\boldsymbol{d}}=\left[1,\exp(-\hat{\theta}),\ldots,\exp(-(N-1)\hat{\theta})\right]^T. \quad (14)$$

Plugging (13) into (7), results in

$$H_{\boldsymbol{\beta}_{\mathrm{CB}},\boldsymbol{\alpha}_{\mathrm{CB}}}=\frac{r\mathrm{D}(\Delta\theta/2,N)\exp(-j(\Delta\phi+(N-1)\Delta\theta/2))}{1-r\mathrm{D}(\Delta\theta/2,N)\exp(-j(\Delta\phi+(N-1)\Delta\theta/2))} \quad (15)$$

where

$$\mathrm{D}(x,N)\triangleq\frac{1}{N}\frac{\sin(Nx)}{\sin(x)}$$

is the normalized Dirichlet kernel and

$$\Delta\theta\triangleq\theta-\hat{\theta},\ \Delta\phi\triangleq\phi-\hat{\phi},\ r\triangleq g/\hat{g},$$

are defined as the DOA, range and gain error terms respectively. In the following, four fundamental scenarios are considered:

1) Perfect alignment ($\Delta\theta=0,\Delta\phi=0$),
2) Steering error ($|\Delta\theta|>0,\Delta\phi=0$),
3) Range error ($\Delta\theta=0,|\Delta\phi|>0$),
4) General ($|\Delta\theta|>0,|\Delta\phi|>0$).

B. The Normalized Beampattern

As commonly done for ULA performance analysis [5], we analyze the normalized response (i.e., where the peak main lobe gain is set to 0_{dB}). Henceforth, setting $\boldsymbol{\beta}_{\mathrm{CB,opt}}=\boldsymbol{\alpha}_{\mathrm{CB,opt}}$, we define the normalized response

$$\mathcal{H}_{\Delta\theta,\Delta\phi,r}\triangleq\frac{H_{\boldsymbol{\beta}_{\mathrm{CB}},\boldsymbol{\alpha}_{\mathrm{CB}}}}{H_{\boldsymbol{\beta}_{\mathrm{CB,opt}},\boldsymbol{\alpha}_{\mathrm{CB,opt}}}}=\frac{H_{\boldsymbol{\beta}_{\mathrm{CB}},\boldsymbol{\alpha}_{\mathrm{CB}}}}{r/(1-r)}, \quad (16)$$

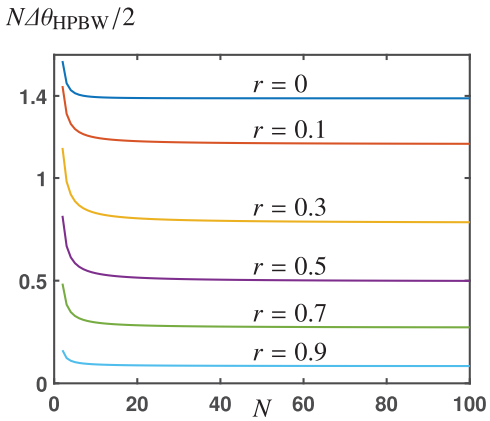

Fig. 4. Plot of $x = N\Delta\theta_{\mathrm{HPBW}}/2$ vs. N, for various r values, obtained by numerically solving (19).

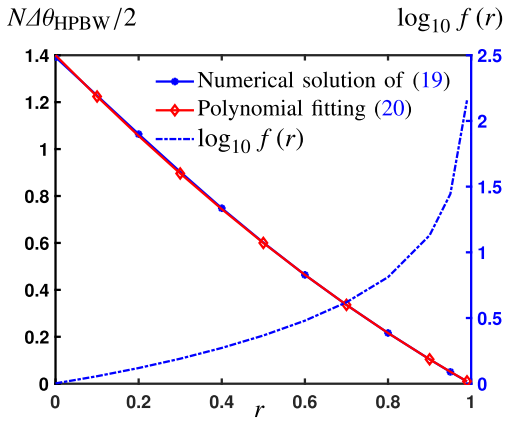

Fig. 5. Evaluation of $N\Delta\theta_{\mathrm{HPBW}}/2$ for $N = 100$ and its approximation $1.4/f(r)$ (marked by red diamonds). $f(r)$ is also presented, in logarithmic scale (dotted curve).

where the $\Delta\theta$, $\Delta\phi$, r subscripts express the DOA, range and gain errors dependency, respectively. Plugging (15) into (16) yields

$$\mathcal{H}_{\Delta\theta,\Delta\phi,r} = \frac{(1-r)\,\mathrm{D}\left(\Delta\theta/2, N\right)}{\exp\left(j\left(\Delta\phi + (N-1)\Delta\theta/2\right)\right) - r\mathrm{D}\left(\Delta\theta/2, N\right)}. \tag{17}$$

Note that the known [5] normalized response of standard ULA is obtained by setting $r = 0$ and $\Delta\phi = 0$

$$\mathcal{H}_{\Delta\theta,\Delta\phi=0,r=0} = \mathrm{D}\left(\Delta\theta/2, N\right)\exp\left(-j\left((N-1)\Delta\theta/2\right)\right).$$

Considering the steering error scenario (i.e., $\Delta\theta \neq 0,\ \Delta\phi = 0$) first, where

$$\mathcal{H}_{\Delta\theta,\Delta\phi=0,r} = \frac{(1-r)\,\mathrm{D}\left(\Delta\theta/2, N\right)}{\exp\left(j\left((N-1)\Delta\theta/2\right)\right) - r\mathrm{D}\left(\Delta\theta/2, N\right)}, \tag{18}$$

we evaluate the FB's beamwidth, sidelobe level and directivity and compare them to those of the standard ULA.

C. Half Power Beamwidth

The half power beamwidth (HPBW), denoted as $\Delta\theta_{\mathrm{HPBW}}$ quantifies the array's main lobe narrowness. It represents the DOA where the beampattern's energy reduces to half of its maximal value. For standard ULA, assuming large N values, it is known [5] that

$$\Delta\theta_{\mathrm{HPBW}}/2 = 1.4/N.$$

In Appendix B we extend this known result for any $r \geq 0$. It turns out that for large N, the HPBW is obtained by solving for x the equality

$$\left(r^2 - 4r + 2\right)\frac{\sin^2(x)}{x^2} + r\frac{\sin(2x)}{x} - 1 = 0 \tag{19}$$

where we define $x \triangleq N\Delta\theta_{HPBW}/2$. In Fig. 4 we plot the numerical solution of (19) for various values of r and N, showing that x reaches its limit around $N = 20$. Also note that for $r = 0$ we obtain the known result of standard ULA with the limiting factor of 1.4. Having the limiting factors for various values of the gain mismatch r, we investigate the feedback related improvement and express the HPBW by

$$\Delta\theta_{\mathrm{HPBW}}/2 \approx \frac{1.4}{f(r)N}.$$

Note that $f(r)$ represents the array aperture improvement factor, compared to the standard ULA. Numerical evaluation (see Fig. 5) shows that $f(r)$ may be approximated with a second order polynomial

$$f(r) \approx \frac{1.4}{(1-r)\left(-0.4r + 1.4\right)}. \tag{20}$$

Note that for an accurate gain match (i.e., $r \to 1$), the RHS of (23) tends towards infinity, implying that the equivalent array has an infinite number of elements ($f(r)N$), hence obtaining perfect spatial selectivity.

D. Sidelobes Attenuation

By taking a derivative of $\mathcal{H}_{\Delta\theta,\Delta\phi=0,r}$ with respect to $\Delta\theta$ it can be easily verified that the beampattern's extrema points are located exactly as in the standard ULA beampattern. Specifically, the sidelobes locations are

$$\Delta\theta_{\mathrm{sidelobe}} = \frac{(2m+1)\,\pi}{N}\ \forall m \in \{\pm 1, \pm 2, \ldots\}. \tag{21}$$

Our main interest is with the first sidelobe (i.e. $m = 1$), therefore we evaluate (18) at $\Delta\theta = 3\pi/N$, which results in

$$\left|\mathcal{H}_{3\pi/N,0,r}\right|^2 = \frac{2\left(1-r\right)^2}{\left(N^2 - 2Nr\right)\left(1 - \cos\left(\frac{3\pi}{N}\right)\right) + 2r^2} \tag{22}$$

and for large N values

$$\lim_{N\to\infty}\left|\mathcal{H}_{3\pi/N,0,r}\right| = \frac{2\left(1-r\right)}{3\pi}.$$

For standard ULA, the gain of the first sidelobe is known to be $2/3\pi$ [5], which implies that the first sidelobe is smaller by a factor of $1 - r$ compared to standard ULA. Specifically, in perfect gain match scenario (i.e., $r \to 1$), the sidelobes vanish.

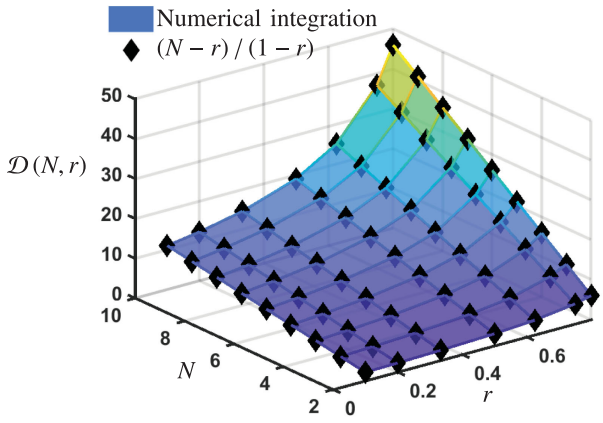

Fig. 6. Plot of $\mathcal{D}(N,r)$, computed using numerical integration (surface), shown to perfectly match the analytic expression (black diamonds) presented in (24). Difference between the numerical integration result and the suggested analytic expression is around $\sim 1e^{-9}$.

TABLE I
PERFORMANCES OF CLASSICAL ULA AND THE PROPOSED FEEDBACK-BEAMFORMING ARCHITECTURE, WITH A GAIN MISMATCH r

	ULA	FEEDBACK BEAMFORMING	IMPROVEMENT
HPBW	$1.4/N$	$1.4/(f(r)N)$	Narrower by a factor of $f(r)$
FIRST SIDELOBE GAIN	$2/3\pi$	$2(1-r)/3\pi$	smaller by a factor of $1-r$ for $N \gg 1$
DIRECTIVITY	N	$(N-r)/(1-r)$	$1/(1-r)$ times higher for $N \gg 1$

E. Array Directivity

The array directivity $\mathcal{D}$ [5], defined as

$$\mathcal{D}(N,r) = \frac{\mathcal{H}_{\Delta\theta=0,\Delta\phi=0,r}}{\frac{1}{2\pi}\int_0^{2\pi}\mathcal{H}_{\Delta\theta,\Delta\phi=0,r}\,d\Delta\theta} = \frac{2\pi}{\int_0^{2\pi}\mathcal{H}_{\Delta\theta,\Delta\phi=0,r}\,d\Delta\theta}, \tag{23}$$

measures the ratio between the maximal array gain at its main-lobe, to the average gain over all directions. For uniformly weighted ULAs with no feedback, it is known [5] that $\mathcal{D}(N,0) = N$. Plugging (18) within (23) and by numerical evaluation (see Fig. 6) we suggest to approximate the directivity with

$$\mathcal{D}(N,r) \approx \frac{N-r}{1-r}, \tag{24}$$

where the standard ULA's known result is obtained for $r=0$. Also, for $N \geq 2$, $\lim_{r\to 1}\mathcal{D}(N,r) = \infty$, implying infinite directivity for the perfectly gain-matched FB.

Finally, expressing the improvement in directivity compared to the standard ULA, assuming large N values, gives rise to

$$\lim_{N\to\infty}\frac{\mathcal{D}(N,r)}{\mathcal{D}(N,0)} = \frac{N/(1-r)}{N} = \frac{1}{1-r}. \tag{25}$$

F. Summary

To conclude this section, we summarize the feedback integration related performance improvements in Table. I

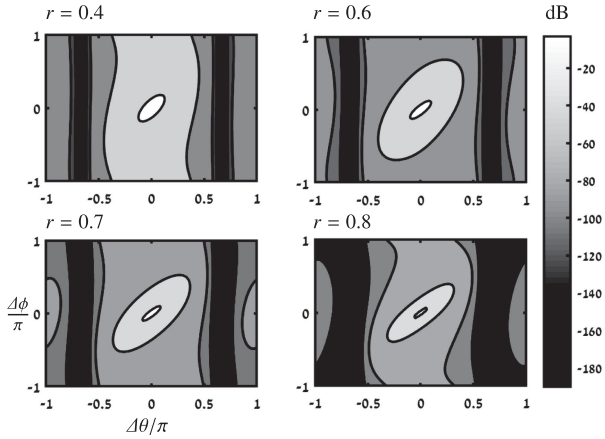

Fig. 7. Evaluation of $10\log_{10}|\mathcal{H}_{\Delta\theta,\Delta\phi,r}|^2$, considering both steer ($\Delta\theta$) and range related ($\Delta\phi$) errors. Centered in each plot, is the 3dB main lobe (white color fill), exemplifying that as the gain mismatch r is set closer to one, we observe an increase of the spatial selectivity (regarding both $\Delta\theta$ and $\Delta\phi$).

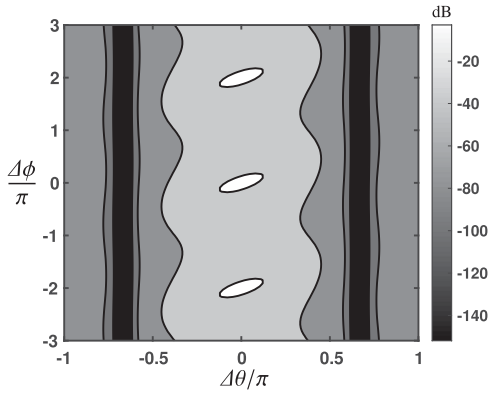

Fig. 8. Evaluation of $10\log_{10}|\mathcal{H}_{\Delta\theta,\Delta\phi,r=0.4}|^2$ for $-3\pi \leq \Delta\phi \leq 3\pi$. The response is 2π periodic.

VI. RANGE ERROR SENSITIVITY

In this section, we investigate $\mathcal{H}_{\Delta\theta,\Delta\phi,r}$ for the general case, where the range misalignment phase term $\Delta\phi$ may also be non zero. In Fig. 7, we plot $|\mathcal{H}_{\Delta\theta,\Delta\phi,r}|$ in logarithmic scale, with respect to both steer and range misalignments. Close inspection of the range error related beampattern behaviour sheds light to some important points. First, we notice that although setting $r \to 1$ (i.e., close to a perfect gain match), sharpens the beampattern's main lobe (i.e., higher spatial selectivity), it also amplifies the range error ($\Delta\phi$) related sensitivity as the main lobe's support over the $\Delta\phi/\pi$ axis shrinks. Next, as evident from (17), the range error related sensitivity is 2π-periodic with respect to $\Delta\phi$ (see Fig. 8). To establish our final observation, we first recall that

$$\phi \triangleq \omega\tau_{pd} = \frac{2\pi R_{\text{rt}}}{\lambda},$$

where $R_{\text{rt}} = 2R$ is the round-trip distance between the array and the target of interest and λ is the wavelength. Define

$$\Delta R_{\text{rt}} = \frac{\Delta\phi\lambda}{2\pi}$$

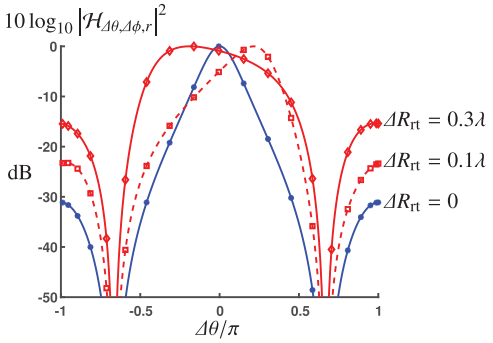

Fig. 9. Evaluation of the array response (where $r = 0.4$) for several values of range error $\Delta R_{\rm rt}$. Even minor range errors significantly distort the beampattern.

to be the range estimation error. Fig. 9 shows that even minor range errors of $\Delta R_{\rm rt} \sim 0.1\lambda$ significantly distort the beampattern.

At first glance, this sensitivity to range errors renders the system being too sensitive for any practical use. This leads us to seek robust implementations, as elaborated in Section VII.

VII. Mitigating Range Error Sensitivity

As demonstrated in the previous section, the beampattern (17) is sensitive to range errors. We now propose an architecture which obtains the desired beampattern $\mathcal{H}_{\Delta\theta,\Delta\phi\to 0,r}$ even for relatively large range errors $\Delta R_{\rm rt}$. Also, we show that the suggested architecture achieves high performance at moderately low signal-to-noise ratio (SNR) scenarios.

A. Intuition

Bearing in mind that the system's phase alignment sensitivity resides in (17) via the term $\exp(j\Delta\phi) = \exp(j\omega\Delta\tau_{pd})$ and that the round-trip delay (τ_{pd}) cannot be controlled, one may suggest to use lower frequencies. Unfortunately, aiming for practical range estimation errors, the transmission of such low frequencies is physically unfeasible. Instead, we suggest simultaneous transmission of several frequencies in order to resolve the range error sensitivity. In the following, we suggest a dual frequency (DF) waveform, utilizing two harmonics, ω_1 and ω_2.

B. Suggested Processing Scheme

In Fig. 10, we demonstrate the use of two independently configured FB instances (see also Fig. 2), where each instance is designed to treat a specific frequency band. A bandpass filter BPF_{ω_i}, $i = 1, 2$ filters a narrowband slice around $\omega_i = 2\pi f_i$. These filters are used to generate both the transmitted feedback signal (Tx_i) and the outputs z_i. The inputs $s_i(t) = \exp(j\omega_i t)$ are the two narrowband stimuli signals and $\text{n}_i(t)$ represents the additive noise.

Note that in the suggested architecture we do not add array elements, but merely double the beamformer processing effort.

For each FB block, its output is given by

$$z_i(t) = H_{\boldsymbol{\beta}_i,\boldsymbol{\alpha}_i}(\omega_i)\exp(j\omega_i t) \quad i \in \{1, 2\},$$

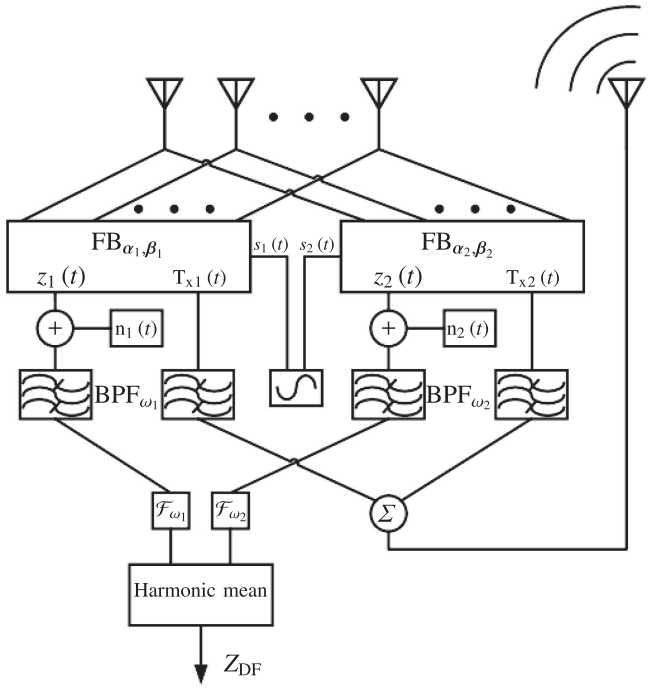

Fig. 10. Dual-frequency beamformer, consisting of two independent FB blocks and narrowband bandpass filters. The blocks marked by $\mathcal{F}_{\omega_i}$ compute the Fourier coefficients in ω_i and their outputs feed the harmonic mean calculator, which generates the DF beamformer's output.

where $\boldsymbol{\beta}_i, \boldsymbol{\alpha}_i$ are the coefficients of the i'th beamformer. Motivated by the desire to mitigate the $\Delta\phi$ dependency of the system, which appears in the denominator of (17)'s RHS, we compute the reciprocal of each frequency response, average, and compute the reciprocal again. This leads to the harmonic mean of both beamformers' outputs (see Fig. 10), which formally, up to a constant term, takes the form

$$Z_{\rm DF} = \left|H^{-1}_{\boldsymbol{\beta}_1\boldsymbol{\alpha}_1}(\omega_1) + H^{-1}_{\boldsymbol{\beta}_2,\boldsymbol{\alpha}_2}(\omega_2)\right|^{-1}. \tag{26}$$

For convenience, we use subscripts instead of formal ω dependency such that $\phi_i \triangleq \phi(\omega_i)$, $g_i \triangleq g(\omega_i)$, $\boldsymbol{d}_i \triangleq \boldsymbol{d}(\omega_i)$. Also, $r_i \triangleq g_i/\hat{g}_i$ is denoted to be the gain mismatch at ω_i.

Theorem 1: Consider the architecture suggested in Fig. 10, and let $\boldsymbol{\alpha}_i$, $\boldsymbol{\beta}_i$ be the coefficients of the i'th FB. Then setting

$$\boldsymbol{\alpha}_1 = \boldsymbol{\beta}_1, \ \boldsymbol{\alpha}_2 = -\boldsymbol{\beta}_2 = \left[1/\hat{g}_2, 0, \ldots, 0\right], \tag{27}$$

results in

$$Z_{\rm DF} = \left|\frac{g_1\boldsymbol{\beta}_1^H\boldsymbol{d}_1}{1 - \left(g_1\boldsymbol{\beta}_1^H\boldsymbol{d}_1/r_2\right)\exp\left(-j\left(\phi_1 - \phi_2\right)\right)}\right|, \tag{28}$$

Proof: See Appendix C.

Assuming close frequencies, $Z_{\rm DF}$ in (28) closely resembles the single frequency (SF) beampattern in (7), where the range related phase ϕ is now replaced by $\phi_1 - \phi_2 = (\omega_1 - \omega_2)\tau_{pd}$. Hence, one may significantly mitigate the range mismatch distortion of the beampattern by selecting close stimuli frequencies. We also note that throughout the development of (28), we did not assume any specific array geometry, hence this result is valid for arbitrary arrays and not just ULA.

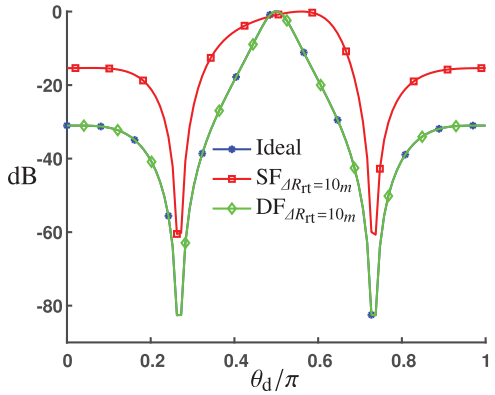

Fig. 11. Simulating a 3 element ULA with $r_1 = 0.6^2$, $r_2 = 0.6$ (hence $\kappa = 0.6$), assuming an infinite SNR. For each target direction θ_d, the DF beamformer output Z_{DF} is evaluated where the beamformer is set to enhance signals impinging from $\theta_d = \pi/2$. The (modulus λ) range error is $\Delta R_{rt} = 0.3\lambda$. The single frequency (SF) beamformer (red squares) and the dual-frequency (DF) solution (green diamonds) are compared to the ideal response $\Delta R_{rt} = 0$ (blue dots) as a reference.

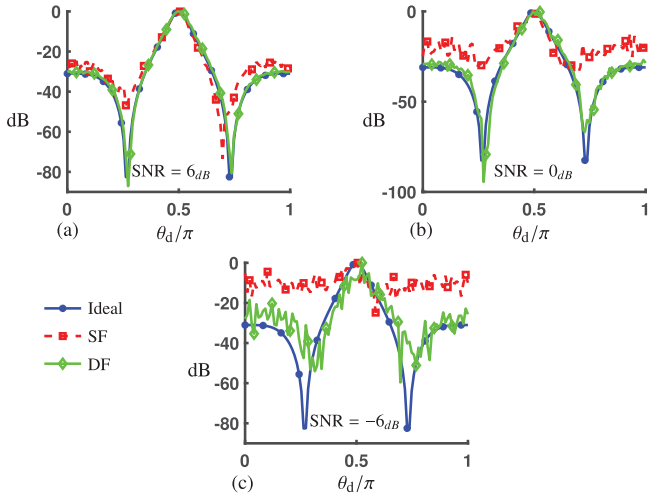

Fig. 12. Directional response of the 3 element ULA, as in Fig. 11, simulated for the noisy scenario. The additive noises $n_1(t)$ and $n_2(t)$ (see Fig. 10), are set to obtain SNRs of 6 dB (a), 0 dB (b) and −6 dB (c).

C. Numerical Example

Consider a radio frequency carrier of 10 GHz and typical range error of $\Delta R_{rt} = 10$ m, which is $333\frac{1}{3}\lambda$ (assuming speed of light, $c = 3 \cdot 10^8$ m/s). The single frequency beampattern distortion, being periodic in λ, will closely resemble the 0.3λ error plot presented in Fig. 9. Assume that we aim to achieve a maximal phase error of $\Delta\phi = 0.01\pi$. Hence, when using the DF architecture, the dictated frequency separation must satisfy

$$\left|(\omega_1 - \omega_2)\frac{\Delta R_{rt}}{c}\right| < 0.01\pi, \tag{29}$$

or equivalently, for a maximal range error of 10 m, a frequency separation of

$$|f_1 - f_2| < 0.005c/\Delta R_{rt} = 150\,\text{kHz}$$

is required.

D. Dual Frequency Simulation

We now simulate (28) for the DF structured FB, generalizing the CB approach and setting

$$\boldsymbol{\beta}_1^* = \frac{-\hat{\boldsymbol{d}}_1^* \exp\left(j\left(\hat{\phi}_1 - \hat{\phi}_2\right)\right)}{\hat{g}_1 \left\|\hat{\boldsymbol{d}}_1\right\|^2}.$$

With this choice, and similarly to (15), (28) becomes

$$H_{DF,CB}(\omega) = \left|\frac{r_1 \mathrm{D}(\Delta\theta/2, N)}{1 - \kappa \mathrm{D}(\Delta\theta/2, N)\exp\left(-j\left(\phi_2 - \phi_1 + (N-1)\Delta\theta/2\right)\right)}\right|, \tag{30}$$

where $\kappa \triangleq r_1/r_2$ is the gain mismatch ratio. For close frequencies, one may assume that $r_1 \approx r_2$, hence κ tends towards unity, thus significantly mitigating the gain mismatch effect even when both feedback beamformers are mismatched.

Simulating the DF architecture, configured to mitigate range estimation errors as in (29) and plotting its normalized (to 0 dB peak gain) beampattern together with the perfectly range aligned scenario, we show in Fig. 11 that the DF architecture achieves a near-optimal performance, despite the inherent range error of $\Delta R_{rt} = 10$ m. In Fig. 12, we repeat the simulation while adding white Gaussian noise to the output of each feedback beamformer. Evidently, even in the noisy case, the DF beamformer achieves a close-to-ideal beampattern, while the SF beamformer suffers from severe distortions.

VIII. Conclusions

Integrating feedback into standard beamformers proved to achieve the spatial domain equivalent of the temporal IIR filtering. It seems that a simple generalization of the conventional-beamformer maximizes (locally) the system's spatial information, thus enabling high localization accuracy. The feedback-based architecture performance evaluation predicts an unlimited improvement in all criteria, when considering perfect knowledge of the target's range and the channel attenuation. It turns out that a single frequency waveform based feedback-beamformer is impractical, being too sensitive to even mild target range estimation errors. Fortunately, using a dual-frequency waveform and applying simple frequency domain manipulations to the output and feedback signals, were found to serve as a low frequency (hence low sensitivity) equivalent of the single frequency scheme. Also, the dual frequency scheme proved to be of low noise sensitivity, featuring high performance even in relatively low signal-to-noise-ratio scenarios.

Future study of the feedback beamforming concept may be applied to other array processing applications other than localization. Furthermore, it is worthwhile to inspect other interesting choices of coefficients rather than the conventional-beamformer generalization, other waveforms and associated processing schemes, to extend the results to dynamic/multiple targets and to consider sensors with general radiation patterns. Also, one may consider generalizing the suggested architecture to multiple-input-multiple-output systems, enabling

a steered/focused (rather than omni-directional) feedback transmission.

APPENDIX A
FIM CALCULATION

Following (9), we elaborate the steps leading to (11). First, we express the partial derivatives of Z with respect to $\boldsymbol{\eta}$, resulting in

$$\begin{aligned}
&\frac{1}{\mathrm{S}}\frac{\partial \mathrm{Z}}{\partial \theta_{\mathrm{d}}} \\
&= \frac{\begin{pmatrix} g\boldsymbol{\beta}^H \boldsymbol{A}\boldsymbol{d}\exp(-j\phi)\left(1-g\boldsymbol{\alpha}^H\boldsymbol{d}\exp(-j\phi)\right) \\ +g^2\boldsymbol{\beta}^H\boldsymbol{d}\boldsymbol{\alpha}^H\boldsymbol{A}\boldsymbol{d}\exp(-2j\phi)\end{pmatrix}}{\left(1-g\boldsymbol{\alpha}^H\boldsymbol{d}\exp(-j\phi)\right)^2} \\
&= \frac{g\boldsymbol{\beta}^H\boldsymbol{A}\boldsymbol{d}\exp(-j\phi)-g^2\boldsymbol{\beta}^H\left(\boldsymbol{A}\boldsymbol{d}\boldsymbol{d}^T-\boldsymbol{d}\boldsymbol{d}^T\boldsymbol{A}\right)\boldsymbol{\alpha}^*\exp(-2j\phi)}{\left(1-g\boldsymbol{\alpha}^H\boldsymbol{d}\exp(-j\phi)\right)^2} \\
&= \frac{g\boldsymbol{\beta}^H\boldsymbol{A}\boldsymbol{d}\exp(-j\phi)+g^2\boldsymbol{\beta}^H\boldsymbol{B}\boldsymbol{\alpha}^*\exp(-2j\phi)}{\left(1-g\boldsymbol{\alpha}^H\boldsymbol{d}\exp(-j\phi)\right)^2}
\end{aligned}$$

and

$$\begin{aligned}
\frac{1}{\mathrm{S}}\frac{\partial \mathrm{Z}}{\partial \phi} &= \frac{\begin{pmatrix} -jg\boldsymbol{\beta}^H\boldsymbol{d}\exp(-j\phi)\left(1-g\boldsymbol{\alpha}^H\boldsymbol{d}\exp(-j\phi)\right) \\ -jg^2\boldsymbol{\beta}^H\boldsymbol{d}\boldsymbol{\alpha}^H\boldsymbol{d}\exp(-2j\phi)\end{pmatrix}}{\left(1-g\boldsymbol{\alpha}^H\boldsymbol{d}\exp(-j\phi)\right)^2} \\
&= \frac{-jg\boldsymbol{\beta}^H\boldsymbol{d}\exp(-j\phi)}{\left(1-g\boldsymbol{\alpha}^H\boldsymbol{d}\exp(-j\phi)\right)^2}
\end{aligned}$$

where we defined $\boldsymbol{B} \triangleq \boldsymbol{d}\boldsymbol{d}^T\boldsymbol{A}-\boldsymbol{A}\boldsymbol{d}\boldsymbol{d}^T$. The main diagonal elements of the FIM are

$$\begin{aligned}
J_{\theta_{\mathrm{d}}\theta_{\mathrm{d}}} &= \Re\left\{\frac{1}{2\pi\sigma^2}\int_{-\omega_s/2}^{\omega_s/2}\left|\frac{\partial \mathrm{Z}}{\partial\theta_{\mathrm{d}}}\right|^2 d\omega\right\} \\
&= \frac{1}{2\pi\sigma^2}\int_{-\omega_s/2}^{\omega_s/2}\frac{\left|g\boldsymbol{\beta}^H\boldsymbol{A}\boldsymbol{d}-g^2\boldsymbol{\beta}^H\boldsymbol{B}\boldsymbol{\alpha}^*\exp(-j\phi)\right|^2}{\left|1-g\boldsymbol{\alpha}^H\boldsymbol{d}\exp(-j\phi)\right|^4}|\mathrm{S}|^2\,d\omega, \\
J_{\phi\phi} &= \Re\left\{\frac{1}{2\pi\sigma^2}\int_{-\omega_s/2}^{\omega_s/2}\left|\frac{\partial \mathrm{Z}}{\partial\phi}\right|^2 d\omega\right\} \\
&= \frac{1}{2\pi\sigma^2}\int_{-\omega_s/2}^{\omega_s/2}\frac{\left|g\boldsymbol{\beta}^H\boldsymbol{d}\right|^2}{\left|1-g\boldsymbol{\alpha}^H\boldsymbol{d}\exp(-j\phi)\right|^4}|\mathrm{S}|^2\,d\omega
\end{aligned}$$

and the cross terms are

$$\begin{aligned}
J_{\theta_{\mathrm{d}}\phi} &= J^*_{\phi\theta_{\mathrm{d}}} \\
&= \Re\left\{\frac{1}{2\pi\sigma^2}\int_{-\omega_s/2}^{\omega_s/2}\left(\frac{\partial \mathrm{Z}}{\partial\phi}\right)^*\frac{\partial \mathrm{Z}}{\partial\theta_{\mathrm{d}}}d\omega\right\} \\
&= \Re\left\{\frac{1}{2\pi\sigma^2}\int_{-\omega_s/2}^{\omega_s/2}\frac{jg^2\boldsymbol{\beta}^T\boldsymbol{d}^*\boldsymbol{\beta}^H\left(\boldsymbol{A}\boldsymbol{d}+g\boldsymbol{B}\boldsymbol{\alpha}^*\exp(-j\phi)\right)}{\left|1-g\boldsymbol{\alpha}^H\boldsymbol{d}\exp(-j\phi)\right|^4}\right. \\
&\qquad \left.\times|\mathrm{S}|^2\,d\omega\right\}.
\end{aligned}$$

Notice that when the weights are proportional to the conjugated steering vector, i.e.,

$$\boldsymbol{\alpha}, \boldsymbol{\beta} \propto \boldsymbol{d}^*,$$

the $\boldsymbol{\beta}^T B\boldsymbol{\alpha}$ term vanishes. Assuming a real input waveform $s(t)$, the function

$$\frac{|\mathrm{S}|^2}{\left|1-g\boldsymbol{\alpha}^H\boldsymbol{d}\exp(-j\phi)\right|^4}$$

is even with respect to ω, and

$$\boldsymbol{\beta}^H\boldsymbol{A}\boldsymbol{d} \propto \boldsymbol{d}^H\boldsymbol{A}\boldsymbol{d} = \sum_{n=0}^{N-1}A_{n,n}\,|\boldsymbol{d}_n|^2 \propto \omega$$

is odd, hence the cross terms vanish.

APPENDIX B
HALF POWER BEAMWIDTH

We now compute the squared norm of (18), equate it to $1/2$ and compute the value of $N\Delta\theta/2$ for large N. To this end, we denote $\gamma \triangleq \Delta\theta/2$, giving rise to

$$\begin{aligned}
\left|\mathcal{H}_{\Delta\theta,\Delta\phi=0,r}(\omega)\right|^2 &= \frac{(1-r)^2\,\mathrm{D}^2(\gamma,N)}{\left|\exp(j(N-1)\gamma)-r\mathrm{D}(\gamma,N)\right|^2} \\
&\overset{N\gg 1}{\approx} \frac{(1-r)^2\,\mathrm{D}^2(\gamma,N)}{1-2r\cos(N\gamma)\mathrm{D}(\gamma,N)+r^2\mathrm{D}^2(\gamma,N)}.
\end{aligned}$$

Equating to $1/2$, leads to

$$\left(r^2-4r+2\right)\mathrm{D}^2(\gamma,N)+2r\cos(N\gamma)\mathrm{D}(\gamma,N)-1=0.$$

Since for large N, the mainlobe beamwidth goes to zero, we approximate $\sin(\gamma)$ with γ. Also defining $x \triangleq N\gamma = N\Delta\theta/2$ we obtain (19).

APPENDIX C
PROOF OF THEOREM 1

Proof: Elaborating (26) gives rise to

$$\begin{aligned}
Z_{\mathrm{DF}}^{-1} &= \left|\frac{1-g_1\boldsymbol{\alpha}_1^H\boldsymbol{d}_1e^{-j\phi_1}}{g_1\boldsymbol{\beta}_1^H\boldsymbol{d}_1e^{-j\phi_1}}+\frac{1-g_2\boldsymbol{\alpha}_2^H\boldsymbol{d}_2e^{-j\phi_2}}{g_2\boldsymbol{\beta}_2^T\boldsymbol{d}_2e^{-j\phi_2}}\right| \\
&= \left|\frac{\begin{pmatrix} g_2\boldsymbol{\beta}_2^H\boldsymbol{d}_2e^{-j\phi_2} \\ -g_1g_2\left(\boldsymbol{\alpha}_1^H\boldsymbol{d}_1\boldsymbol{\beta}_2^H\boldsymbol{d}_2+\boldsymbol{\alpha}_2^H\boldsymbol{d}_2\boldsymbol{\beta}_1^H\boldsymbol{d}_1\right)e^{-j(\phi_1+\phi_2)} \\ +g_1\boldsymbol{\beta}_1^H\boldsymbol{d}_1e^{-j\phi_1}\end{pmatrix}}{g_1\boldsymbol{\beta}_1^H\boldsymbol{d}_1g_2\boldsymbol{\beta}_2^H\boldsymbol{d}_2}\right| \\
&= \left|\frac{g_2\boldsymbol{\beta}_2^H\boldsymbol{d}_2e^{j(\phi_1-\phi_2)}+g_1\boldsymbol{\beta}_1^H\boldsymbol{d}_1}{g_1\boldsymbol{\beta}_1^H\boldsymbol{d}_1g_2\boldsymbol{\beta}_2^H\boldsymbol{d}_2}\right. \\
&\qquad \left.-\frac{\left(\boldsymbol{\beta}_1^H\boldsymbol{d}_1\boldsymbol{\alpha}_2^H\boldsymbol{d}_2+\boldsymbol{\beta}_2^H\boldsymbol{d}_2\boldsymbol{\alpha}_1^H\boldsymbol{d}_1\right)e^{-j\phi_2}}{\boldsymbol{\beta}_1^H\boldsymbol{d}_1\boldsymbol{\beta}_2^H\boldsymbol{d}_2}\right|.
\end{aligned}$$

Note that in the special case of choosing $\boldsymbol{\alpha}_1 = \boldsymbol{\beta}_1,\ \boldsymbol{\alpha}_2 = -\boldsymbol{\beta}_2$, the resultant beampattern simplifies to

$$Z_{\mathrm{DF}} = \left| \frac{g_1 \boldsymbol{\beta}_1^H \boldsymbol{d}_1}{1 + \frac{g_1 \boldsymbol{\beta}_1^H \boldsymbol{d}_1}{g_2 \boldsymbol{\beta}_2^H \boldsymbol{d}_2} \exp\left(-j\left(\phi_1 - \phi_2\right)\right)} \right|.$$

Also setting $\boldsymbol{\beta}_2 = [-1/\hat{g}_2, 0, \ldots, 0]$ results in (28). ■

ACKNOWLEDGMENT

The authors thank the anonymous reviewers for their constructive comments which helped to improve the presentation of this paper.

REFERENCES

[1] M. Skolnik, *Radar Handbook*, 3rd ed., Electronics Electrical Engineering, New York, NY, USA: McGraw-Hill Education, 2008.
[2] T. Long, J. Chen, G. Huang, J. Benesty, and I. Cohen, "Acoustic source localization based on geometric projection in reverberant and noisy environments," *IEEE J. Sel. Topics Signal Process*, vol. 13, no. 1, pp. 482–495, Mar. 2019.
[3] P. Comon, "Independent component analysis, a new concept?," *Signal Process.*, vol. 36, no. 3, pp. 287–314, 1994.
[4] S. Verdu *et al.*, *Multiuser Detection*. Cambridge, U.K.: Cambridge Univ. Press, 1998.
[5] H. L. Van Trees, *Optimum Array Processing: Part IV of Detection, Estimation, and Modulation Theory*. Hoboken, NJ, USA: Wiley, 2004.
[6] J. Benesty, I. Cohen, and J. Chen, *Fundamentals of Signal Enhancement and Array Signal Processing*. Singapore: Wiley-IEEE Press, 2018.
[7] R. Schmidt, "Multiple emitter location and signal parameter estimation," *IEEE Trans. Antennas Propag.*, vol. AP-34, no. 3, pp. 276–280, Mar. 1986.
[8] P. Pal and P. Vaidyanathan, "Nested arrays: A novel approach to array processing with enhanced degrees of freedom," *IEEE Trans. Signal Process.*, vol. 58, no. 8, pp. 4167–4181, Aug. 2010.
[9] P. Chevalier, L. Albera, A. Ferréol, and P. Comon, "On the virtual array concept for higher order array processing," *IEEE Trans. Signal Process.*, vol. 53, no. 4, pp. 1254–1271, Apr. 2005.
[10] M. C. Dogan and J. M. Mendel, "Applications of cumulants to array processing. i. aperture extension and array calibration," *IEEE Trans. Signal Process.*, vol. 43, no. 5, pp. 1200–1216, May 1995.
[11] P. Chevalier, A. Ferréol, and L. Albera, "High-resolution direction finding from higher order statistics: The $2rmq$-music algorithm," *IEEE Trans. Signal Process.*, vol. 54, no. 8, pp. 2986–2997, Aug. 2006.
[12] A. Moffet, "Minimum-redundancy linear arrays," *IEEE Trans. Antennas Propag.*, vol. AP-16, no. 2, pp. 172–175, Mar. 1968.
[13] S. U. Pillai, Y. Bar-Ness, and F. Haber, "A new approach to array geometry for improved spatial spectrum estimation," *Proc. IEEE*, vol. 73, no. 10, pp. 1522–1524, 1985.
[14] S. Pillai and F. Haber, "Statistical analysis of a high resolution spatial spectrum estimator utilizing an augmented covariance matrix," *IEEE Trans. Acoust. Speech, Signal Process.*, vol. ASSP-35, no. 11, pp. 1517–1523, Aug. 1987.
[15] E. Kupershtein, M. Wax, and I. Cohen, "Single-site emitter localization via multipath fingerprinting," *IEEE Trans. Signal Process.*, vol. 61, no. 1, pp. 10–21, Jan. 2013.
[16] O. L. Frost, "An algorithm for linearly constrained adaptive array processing," *Proc. IEEE*, vol. 60, no. 8, pp. 926–935, 1972.
[17] D. G. Manolakis *et al.*, *Statistical and Adaptive Signal Processing: Spectral Estimation, Signal Modeling, Adaptive Filtering, and Array Process*. New York, NY, USA: McGraw-Hill, 2000.
[18] B. D. Van Veen and K. M. Buckley, "Beamforming: A versatile approach to spatial filtering," *IEEE ASSP Mag.*, vol. 5, no. 2, pp. 4–24, Apr. 1988.
[19] F. Wen, B. P. Ng, and V. V. Reddy, "Extending the concept of IIR filtering to array processing using approximate spatial IIR structure," *Multidimensional Syst. Signal Process.*, vol. 24, no. 1, pp. 157–179, Oct. 2013.
[20] L. Bruton and N. Bartley, "Highly selective three-dimensional recursive beam filters using intersecting resonant planes," *IEEE Trans. Circuits Syst.*, vol. CAS-30, no. 3, pp. 190–193, Mar. 1983.
[21] M. A. Woodbury, "Inverting modified matrices," *Memorandum Report*, vol. 42, no. 106, p. 336, Jun. 1950.
[22] A. Zeira and A. Nehorai, "Frequency domain cramer-rao bound for Gaussian processes," *IEEE Trans. Acoustics, Speech, Signal Process.*, vol. 38, no. 6, pp. 1063–1066, Jun. 1990.

Itay Yehezkel Karo received the B.Sc. degree in electrical engineering from the Technion-Israel Institute of Technology, Haifa, Israel, in 2013. From 2010 to 2019, he worked at the Rafael Company, Haifa, Israel. His research interests are signal processing, digital filters, sensor array design and spatial processing. In the spatial processing field of research, he focuses on beamforming, beamsteering and localization.

Tsvi G. Dvorkind received the B.Sc. degree (*summa cum laude*) in computer engineering, the M.Sc. degree (summa cum laude) in electrical engineering, and the Ph.D. degree in electrical engineering from the Technion – Israel Institute of Technology, Haifa, Israel, in 2000, 2003, and 2007, respectively. From 1998 to 2000, he worked at the Electro-Optics Research & Development Company at the Technion, and during 2000-2001 at the Jigami Corporation. He is now with the Rafael Company, Haifa, Israel. His research interests include speech enhancement and acoustical localization, general parameter estimation problems, and sampling theory.

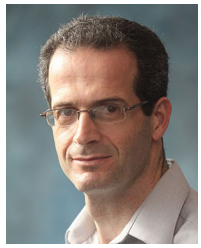

Israel Cohen (Fellow, IEEE) received the B.Sc. (*summa cum laude*), M.Sc., and Ph.D. degrees in electrical engineering from the Technion – Israel Institute of Technology, Haifa, Israel in 1990, 1993, and 1998, respectively.

He is currently the Louis and Samuel Seidan Professor in electrical engineering at the Technion – Israel Institute of Technology. He is also a Visiting Professor at Northwestern Polytechnical University, Xi'an, China. From 1990 to 1998, he was a Research Scientist with RAFAEL Research Laboratories, Haifa, Israel Ministry of Defense. From 1998 to 2001, he was a Postdoctoral Research Associate with the Computer Science Department, Yale University, New Haven, CT, USA. In 2001, he joined the Electrical Engineering Department of the Technion. He is a coeditor of the Multichannel Speech Processing Section of the *Springer Handbook of Speech Processing* (Springer, 2008), and the coauthor of *Fundamentals of Signal Enhancement and Array Signal Processing* (Wiley-IEEE Press, 2018). His research interests are array processing, statistical signal processing, deep learning, analysis and modeling of acoustic signals, speech enhancement, noise estimation, microphone arrays, source localization, blind source separation, system identification and adaptive filtering.

Dr. Cohen was the recipient of the Norman Seiden Prize for Academic Excellence (2017), the SPS Signal Processing Letters Best Paper Award (2014), the Alexander Goldberg Prize for Excellence in Research (2010), and the Muriel and David Jacknow Award for Excellence in Teaching (2009). He is an Associate Member of the IEEE Audio and Acoustic Signal Processing Technical Committee, and Distinguished Lecturer of the IEEE Signal Processing Society. He was an Associate Editor of the IEEE TRANSACTIONS ON AUDIO, SPEECH, AND LANGUAGE PROCESSING and IEEE SIGNAL PROCESSING LETTERS and a Member of the IEEE Audio and Acoustic Signal Processing Technical Committee and the IEEE Speech and Language Processing Technical Committee.